International Journal of Engineering Research and Reviews ISSN 2348-697X (Online)
Vol. 4, Issue 3, pp: (8-28), Month: July - September 2016, Available at: www.researchpublish.com

Structural and Thermal Analysis On A Re-entry Vehicle Aeroshell

Sai Nandyala[1], Sneha Srinivasan[2], Sonali Ravikumar[3]

[1]Student of Aerospace Engineering at SRM University, Kattankulathur, India
[2] Student of Aerospace Engineering at SRM University, Kattankulathur, India
[3] Student of Aerospace Engineering at SRM University, Kattankulathur, India

Abstract: **Hypersonic Inflatable Aerodynamic Decelerator or HIAD is a simple re-entry vehicle designed by NASA. The vehicle happens to be the first of its kind as it inflates after reaching a certain height, making it more feasible to increase payload and ease deceleration. There have been three IRVE (Inflatable Re-entry Vehicle Experiments) designs that have been launched to the tip of the stratosphere to test this new concept out. As this concept is going to be applied in hypersonic speeds, the stresses, heat and pressure on it will be very high. Here, a structural, thermal and thermo structural analysis using different software over the nose of the structure has been performed to try and understand its behaviour at such high speeds and temperatures.**

Keywords: **Re-entry Vehicle, Hypersonic Speed, Hypersonic Inflatable Aerodynamic Vehicle (HIAD), Structural Analysis, Thermal Analysis, Kevlar, Kapton.**

NOMENCLATURE

ρ_∞ → Free-Stream Density,

T_∞ → Free-Stream Static Temperature

M_∞ → Free-Stream Mach Number,

γ → Specific Heat Ratio

R → Specific Gas Constant,

CATIA → Computer Aided Three-Dimensional Interactive Application

CFD → Computational Fluid Dynamics,

IRVE → Inflatable Re-entry Vehicle Experiment

I. INTRODUCTION

Hypersonic Inflatable Aerodynamic Decelerator or HIAD is a simple re-entry vehicle fabricated by NASA under the Inflatable Re-entry Vehicle Experiment (IRVE) conducted by the team to test re-entry vehicles under various conditions and possibly find it feasible for the purpose of traveling to Mars. The vehicle is known to have the capacity to land rovers and systems and instruments onto the Red Planet. It will travel at hypersonic speeds during re-entry phase and requires an in-depth study upon the heat generation by the high temperatures, the physical stresses, the ionization of the particles around the vehicle, and the load it carries along with its aerodynamic effects to generate lift and drag when required.

Here the concern is with the structural and thermal variation of stresses and temperatures separately and with reference to each other under various cases through an analysis under a set of ideal and assumed conditions which can be a factor of the reality and its environment. The vehicle's nose or commonly known as the aero-shell experiences the highest temperatures and pressures at stagnation conditions. First the entire vehicle and a separate aero-shell nose were designed. The inputs of the vehicle's environmental performance parameters are taken from relevant papers and used for the structural analysis.

The structural analysis was performed for various Mach numbers (2, 4, 6 and 8) on the material Kevlar which is used on the outer layer as it takes a high amount of structural load. The thermal analysis was performed on Kapton and further a thermo structural analysis is performed on an assembly of both Kevlar and Kapton.

II. SOFTWARE

The main purpose of the experiment is analysis in terms of thermal, structural, and thermo-structural. To get the basic analysis, a design has to be performed. In all the cases and analysis, the design of the Hypersonic Inflatable Aerodynamic Decelerator Re-entry vehicle and the Aero-shell nose of the vehicle were designed using the software CATIA V5 by Dassault Systemes. The main analysis platform of the experiment was conducted by ANSYS under its Workbench modes. Under the ANSYS Workbench mode, the subsection of Static Structural software was used for the structural analysis, the subsection of Steady-State Thermal was used for the thermal analysis, and the chain of Transient-Thermal and Static Structural subsections were used for the thermo-structural analysis.

ANSYS Static Structural is a mode where structural analysis can be performed over various bodies. The structural analysis of the Kevlar material was conducted using this software. ANSYS Steady-State Thermal was used for the thermal analysis performed on the material Kapton in this report. ANSYS Transient-Thermal coupled with ANSYS Static Structural was performed with a purpose of a thermo-structural analysis over the layered material of Kapton and Kevlar under a contact. This analysis was performed with Transient-Thermal first and the results were the input parameters for the Static Structural mode. Together, they formulated a phase of thermal stresses over the material imported from CATIA.

III. DESIGN

A. Designing of Re-entry Vehicle

The basic design of the 3D model of the re-entry vehicle has been taken with respect to the prior IRVE designs [12]. The dimensions were taken and the design was created.

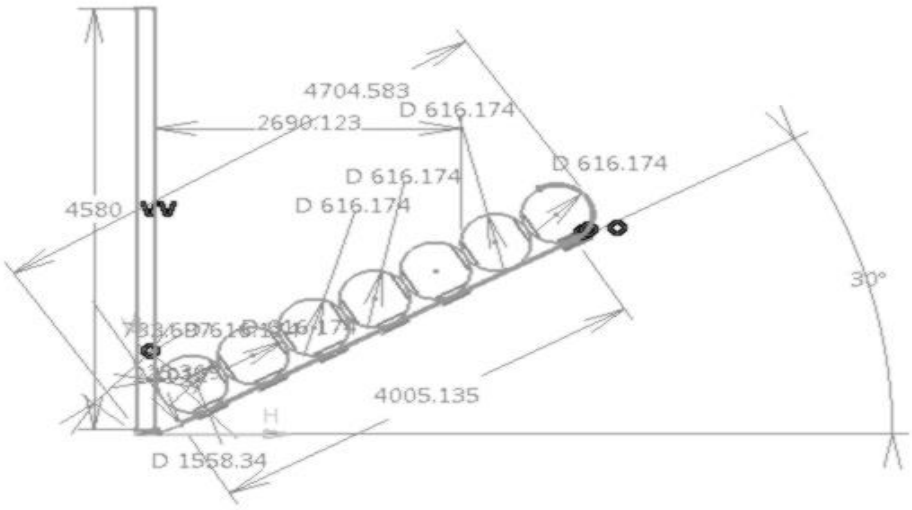

Figure 1: HIAD Re-entry Vehicle Dimensions

Angle of inclination: 30 degrees

Diameter of the inner circles: 616.714 mm

Diameter of the outer inclined curve: 1558.714mm

Height of the column: 4580 mm

Width of the column: 160.57 mm

Full length of the outer curve: 4704.583 mm

The vehicle is lined with 7 layers of torus inside, which is filled with nitrogen when inflated. The central column is designated to electronics and payload.

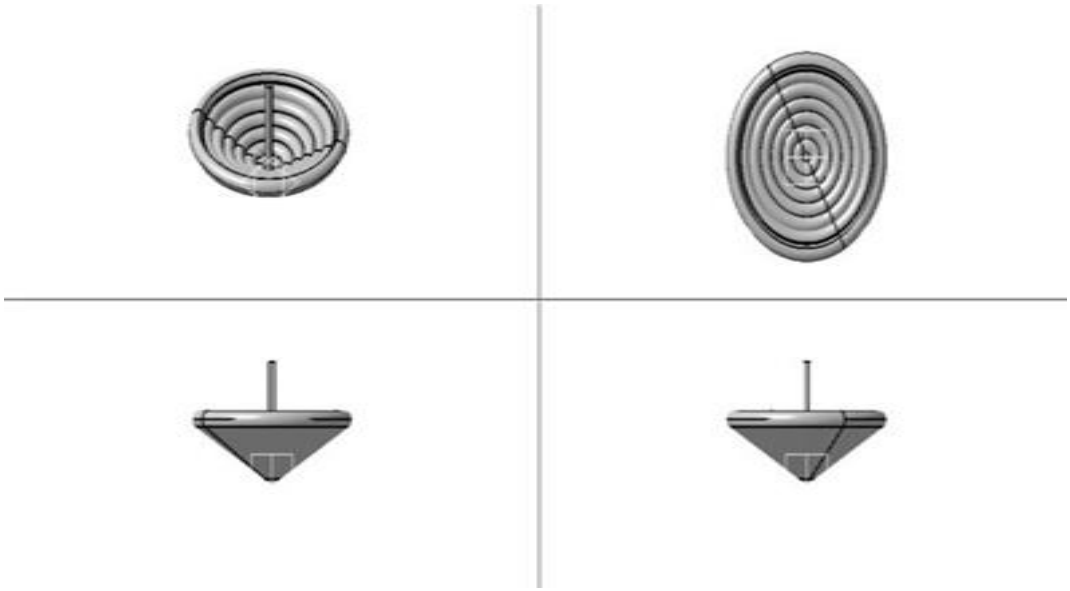

Figure 2: Isometric and 3-View Diagram

B. Designing the Kevlar Nose

Figure 3: Kevlar Nose Dimensions

Dimensions for Kevlar:
Width: 5mm
Radius of the curve: 912.4 mm
Length of the curve: 328.1 mm

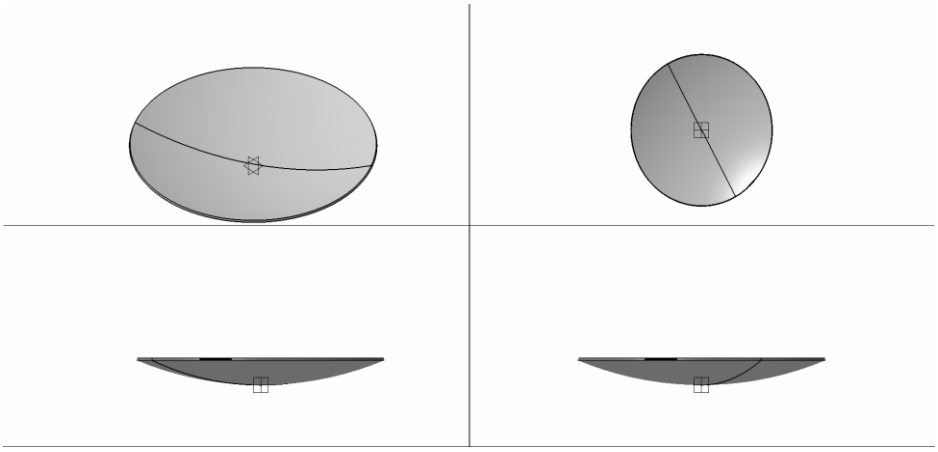

Figure 4: Kevlar Nose 3-View Diagram

Kevlar is mainly used for structural reasons as it has great mechanical properties to resist large amounts of pressures acting on it, making it ideal in re-entry vehicles and space shuttles.

C. Designing Kapton Nose

Figure 5: Kapton Nose Dimensions

Dimensions for Kapton:
Width: 1mm
Radius of the curve: 912.4 mm
Length of the curve: 328.1 mm

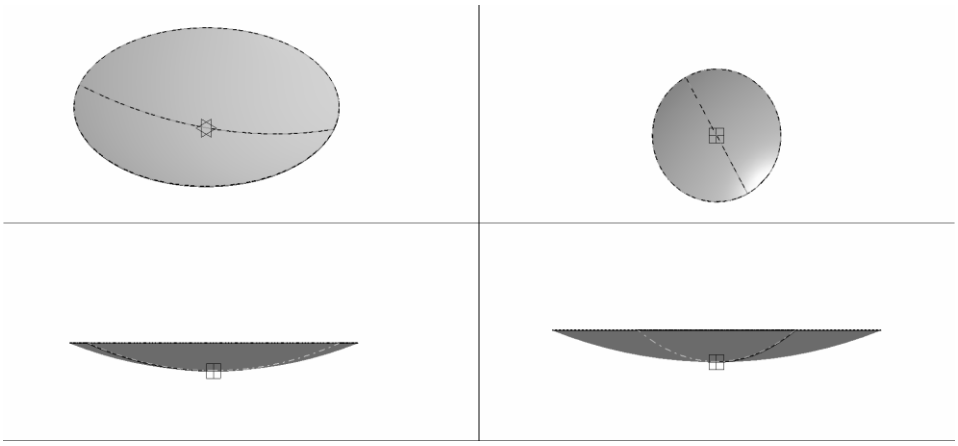

Figure 6: Kapton Nose 3-View

Kapton is a gas barrier material and is usually one of the first layers that come in contact with the high pressures and temperatures on the re-entry vehicle in action. Hence, this is analysed in terms of thermal by itself and thermo-structural layered with Kevlar.

A. Kapton-Kevlar Assembly

Both the geometries are imported into the assembly and are given contact constraint. KAPTON is the outer layer while KEVLAR is the inner layer.

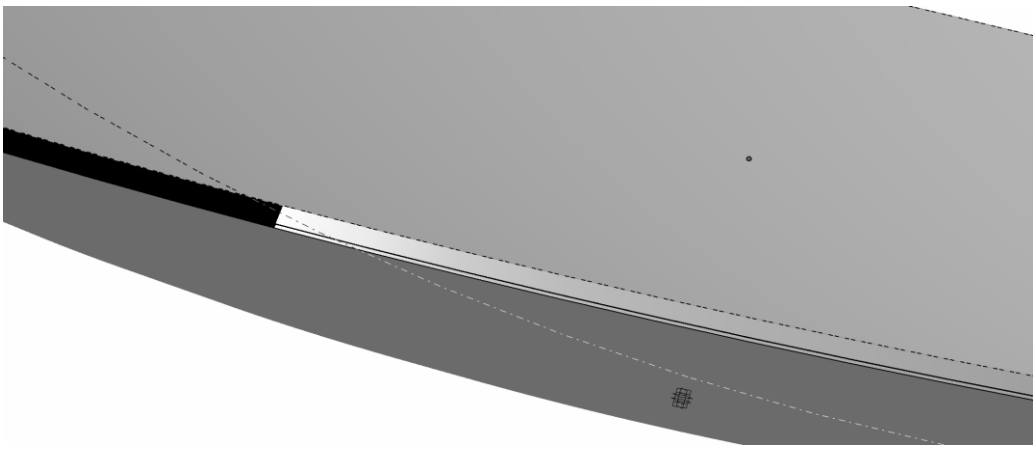

Figure 7: Contact between Kapton and Kevlar

This layered material is used for the thermo-structural analysis.

IV. PERFORMANCE PARAMETERS AND INPUTS

According to the literature survey on Numerical Study of Compressible Flow Past a Re-entry Vehicle Nose by Bianca Szasz published in the U.P.B. Sci. Bull, Series D, Vol. 75, Iss. 4, 2013, [Ref: 24] the solution for the compressible flow past a re-entry vehicle was performed by the Computational Fluid Dynamics using ANSYS Fluent software. This report takes the free stream values of the air at sea level under the following conditions:

Table 1: Input Conditions for CFD Analysis

Free-stream Density ($\rho\infty$)	1.225 [$kg/m3$]
Free-stream Static Temperature (∞T)	288 [$°K$]
Free-stream Mach Number (∞M)	2, 4, 6, 8
Gamma (γ)	1.4
Gas Constant (R)	287 [J/ ($kg°K$)]

The model of the vehicle was set up to be like the picture below where the wall represents the nose of the re-entry vehicle and the remaining walls represent the boundary of the fluid flow. This geometry was meshed with an account of 70780 faces, 35200 cells, and 35581 nodes. The system was set up and the resulting pressure values are given in Table 2.

Table 2: Stagnation Pressure Results

Pressure Results:	
Mach Number	**Stagnation Pressure (Pa)**
2	5.733e+005
4	2.215e+006
6	4.927e+006
8	9.992e+006

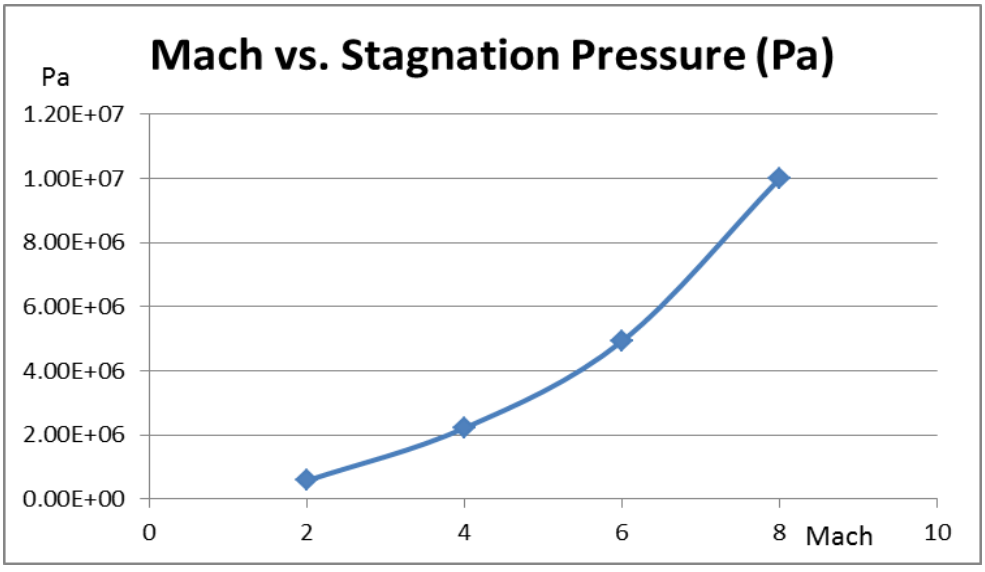

Figure 8: Mach vs. Stagnation Pressure

The graph above seems to be growing at an exponential rate and as the Mach increases further, under ideal conditions; the stagnation pressure should also increase exponentially.

The temperature distribution under the set Cp value at Mach 2 is resulted according to the setup. The highest temperature is analysed to be nearly 515.6 Kelvin at the nose of the body. The temperature distribution under the set Cp value at Mach 8 is resulted according to the setup. The highest temperature is analysed to be nearly 2943 Kelvin at the nose of the body.

The analysis on the material is performed separately for thermal analysis (Kapton) and structural analysis (Kevlar). Then, the combined Kapton and Kevlar layers are analysed under thermal and thermo-structural cases. The combination of the materials has the dimensions and parameters mentioned below.

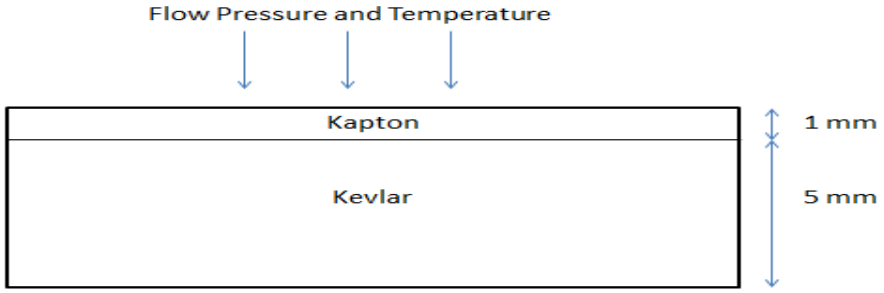

Figure 8: Kapton-Kevlar Layer

The bottom table represents the structural properties of the materials chosen.

Table 3: Structural Properties of Kevlar and Kapton

Material	Kevlar	Kapton
Poisson's Ratio	0.36	0.34
Density (kg/m^3)	1400	1420
Young's Modulus (GPa)	70.5	2.5
Tensile Strength (MPa)	2757	231

The bottom picture represents the thermal properties of the materials chosen.

Table 4: Thermal Properties of Kevlar and Kapton

Thermal Properties:	
Material:	**Isotropic Thermal Conductivity (W/mK)**
Kevlar	0.04
Kapton	0.12

V. ANALYSIS OUTLINE

There are three cases of analysis as mentioned previously. The first case is the simple Static Structural analysis for the Kevlar material.

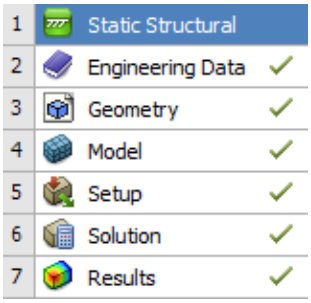

Figure 9: Kevlar Static Structural Process

The second case is the Steady-State Thermal Analysis for the Kapton alone.

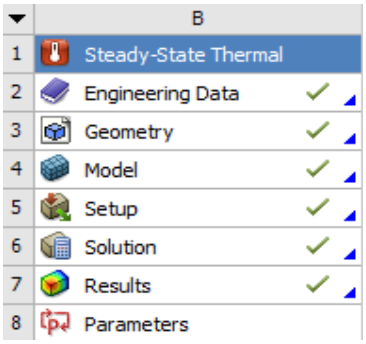

Figure 10: Kapton Steady-State Thermal Process

The last case is for the combination of the transient thermal and static structural to obtain a thermo-structural deformation results.

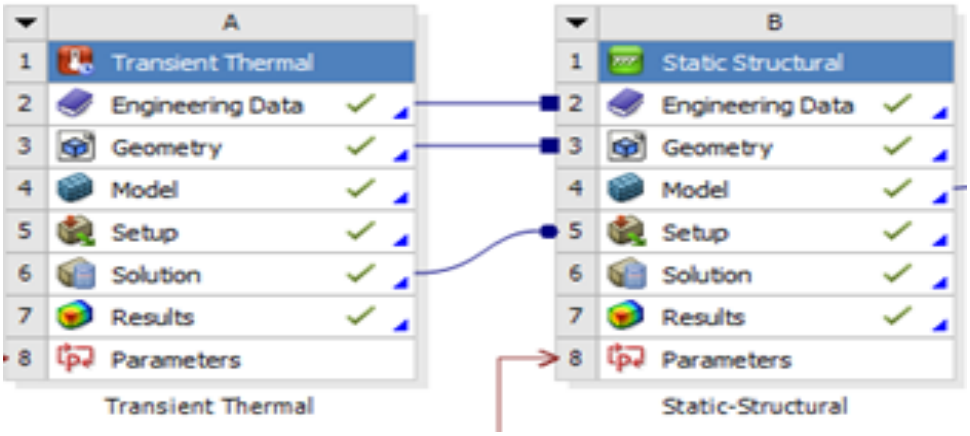

Figure 11: Kapton-Kevlar Thermo-Structural Process

VI. SIMULATION

A. Case 1: Structural Analysis on Kevlar for Mach 2 4, 6, and 8

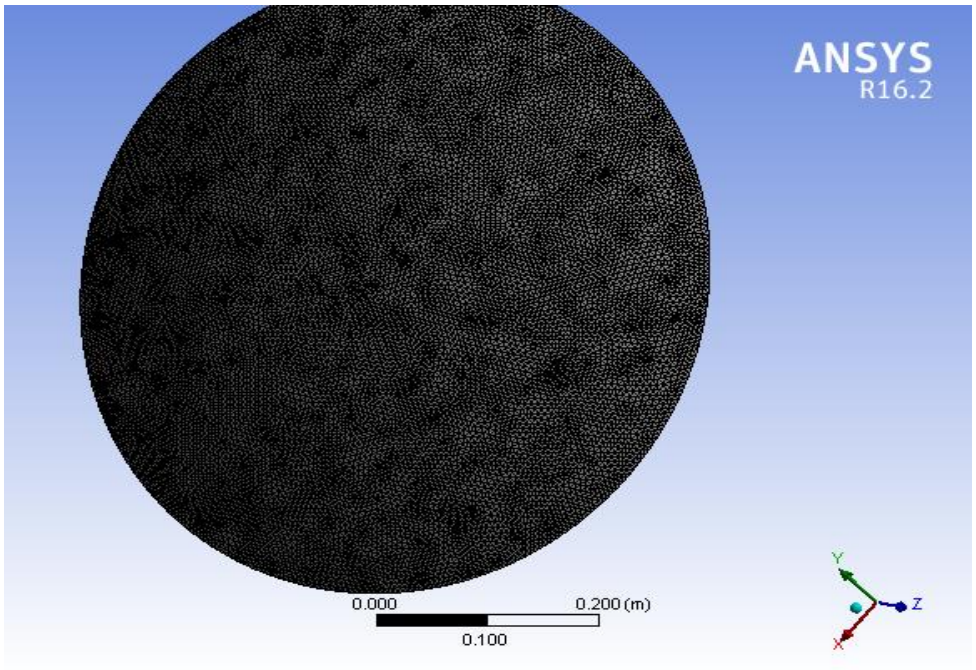

Figure 12: Meshed Kevlar

Total Nodes	184922
Total Elements	92665
Total Body Elements	92665

Figure 13: Mesh Details

A pressure of 5.733e+005 Pa is the input given as the pressure loading at the outer face of the nose as per the category of Mach 2 from the reference taken. In addition, a fixed support is provided on the rim of the Kevlar Aero-shell as it is fixed to the entire body of the re-entry vehicle.

The analysis Total Deformation, total Elastic Strain, and the Equivalent Von-Mises Stress is computed each of the Mach values and pressure values.

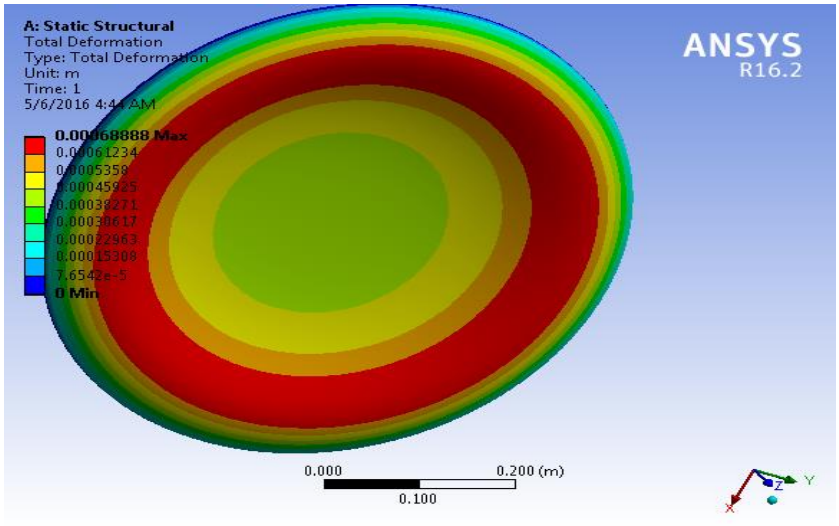

Figure 14: Total Deformation at Mach 2

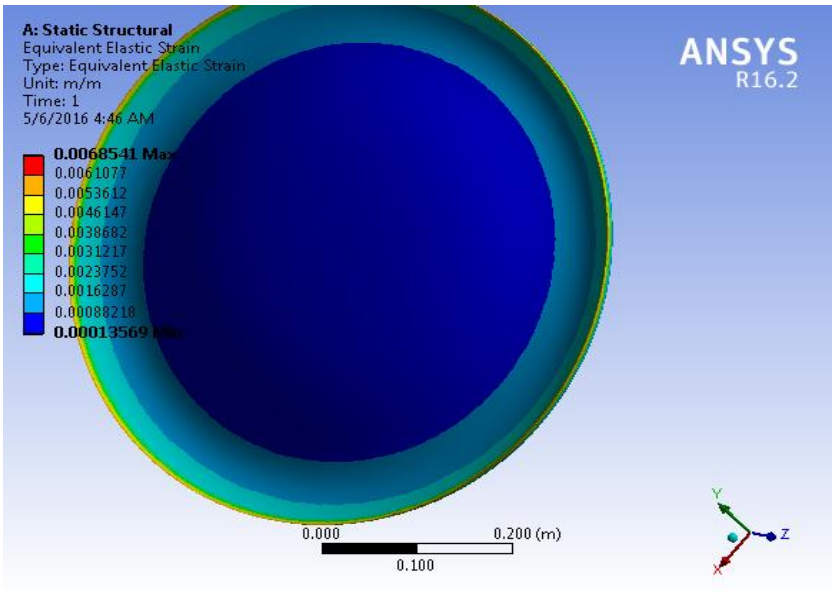

Figure 15: Equivalent Elastic Strain at Mach 2

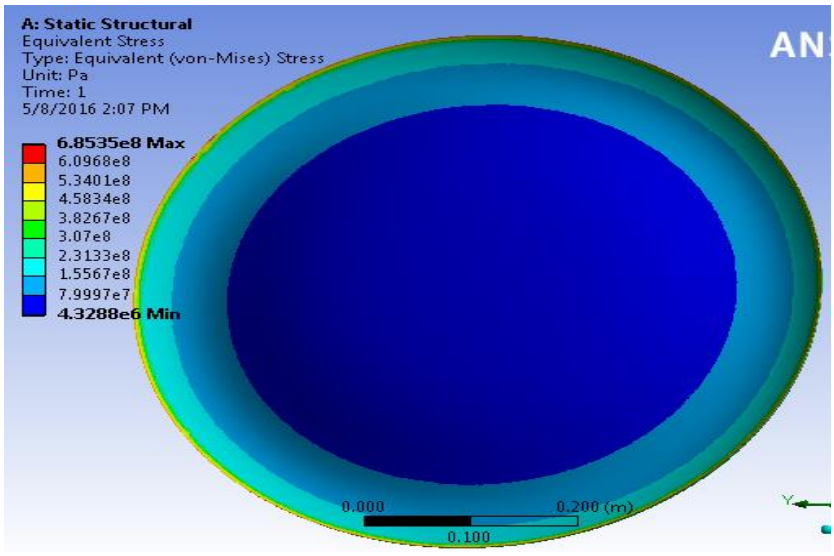

Figure 16: Equivalent Von-Mises Stress at Mach 2

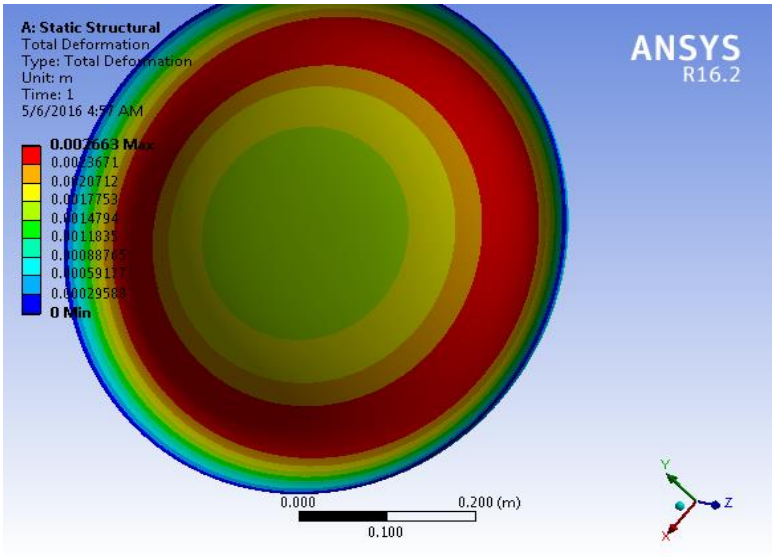

Figure 17: Total Deformation at Mach 4

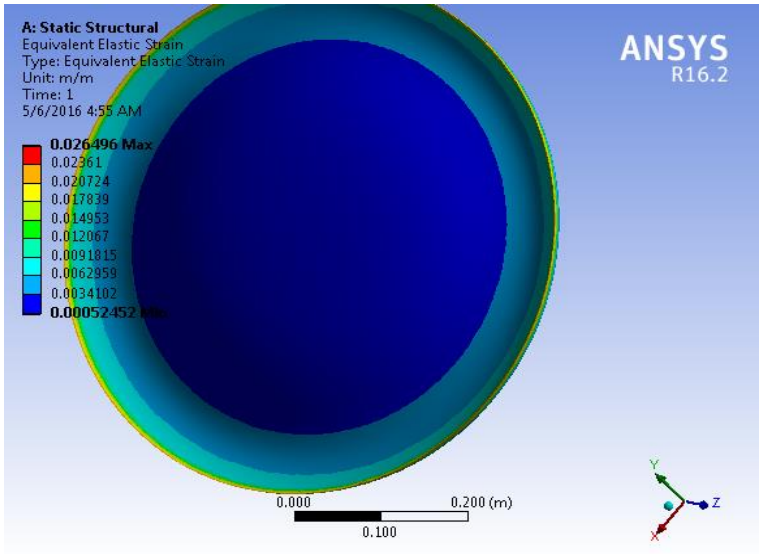

Figure 18: Equivalent Elastic Strain at Mach 4

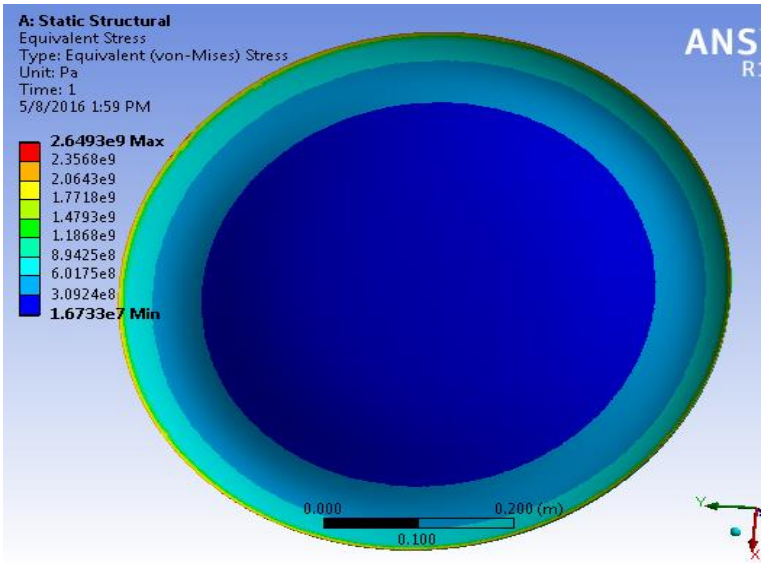

Figure 19: Equivalent Von-Mises Stress at Mach 4

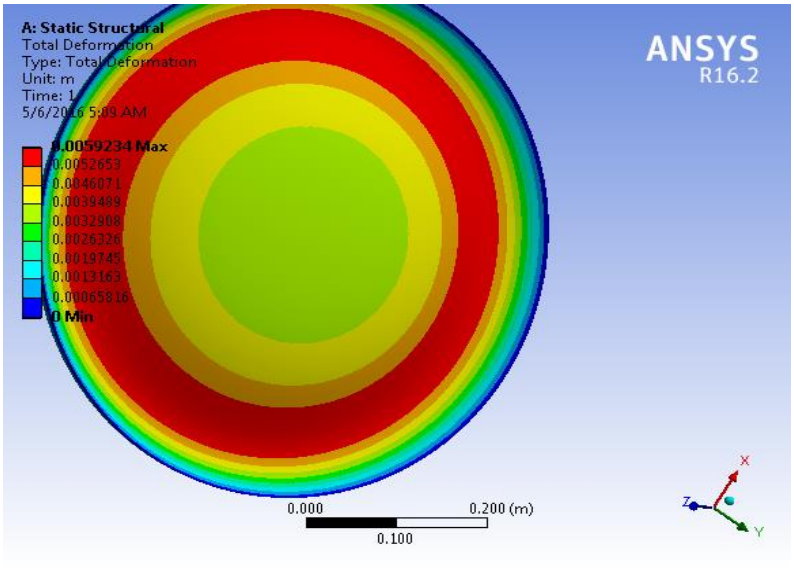

Figure 20: Total Deformation at Mach 6

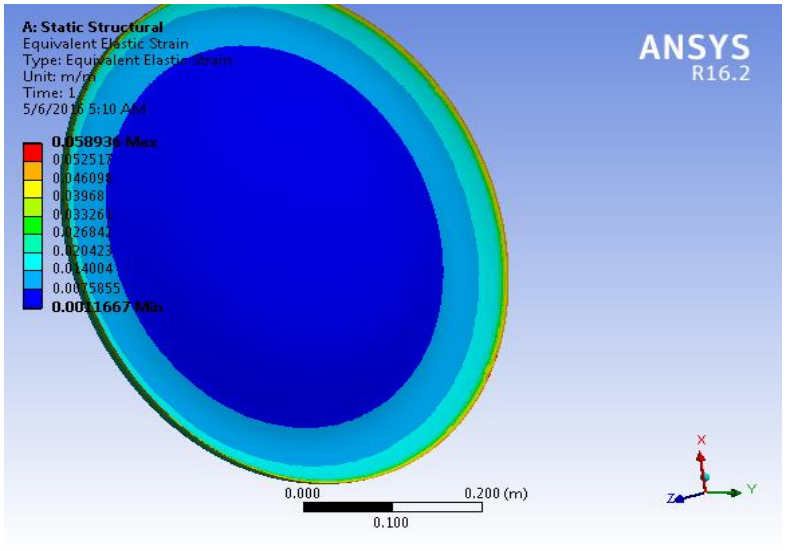

Figure 21: Equivalent Elastic Strain at Mach 6

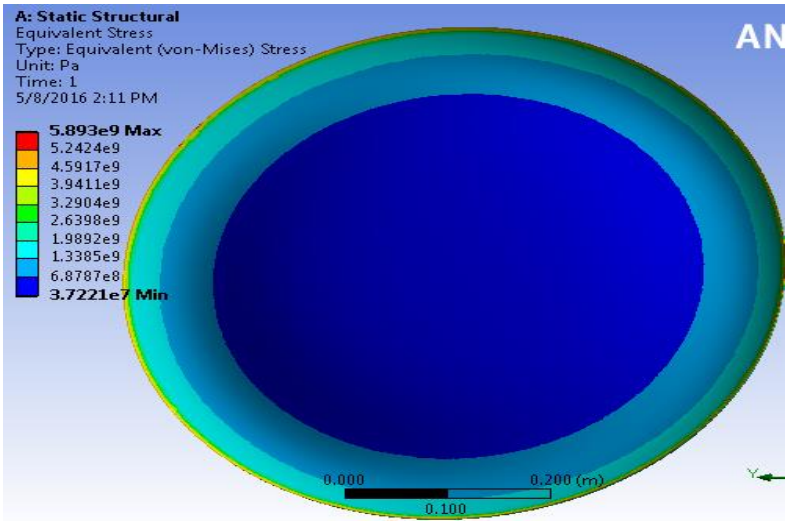

Figure 22: Equivalent Von-Mises Stress at Mach 6

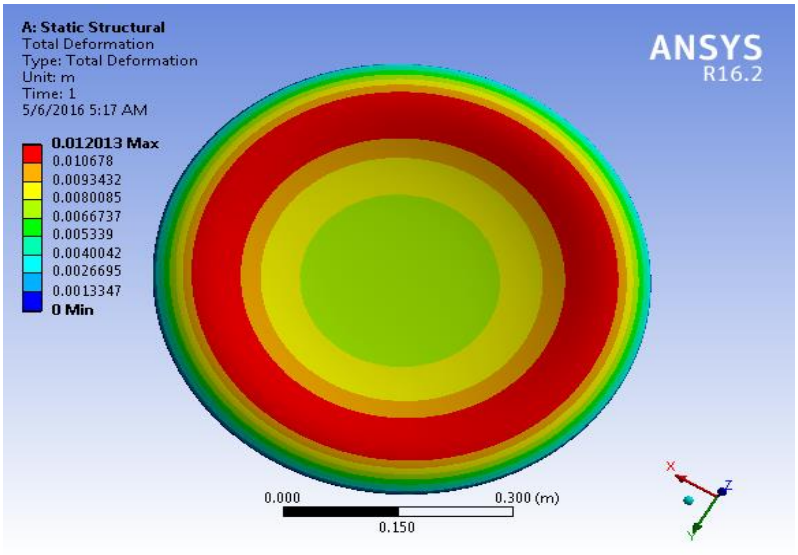

Figure 23: Total Deformation at Mach 8

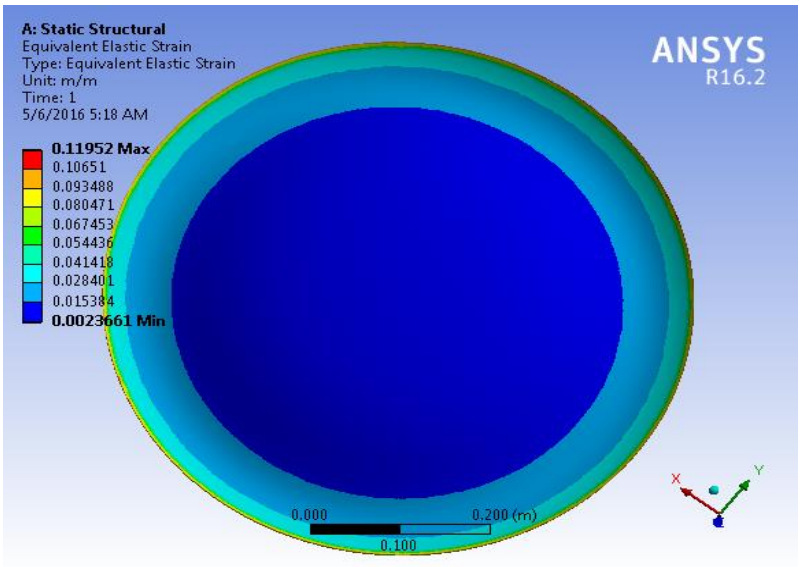

Figure 24: Equivalent Elastic Strain at Mach 8

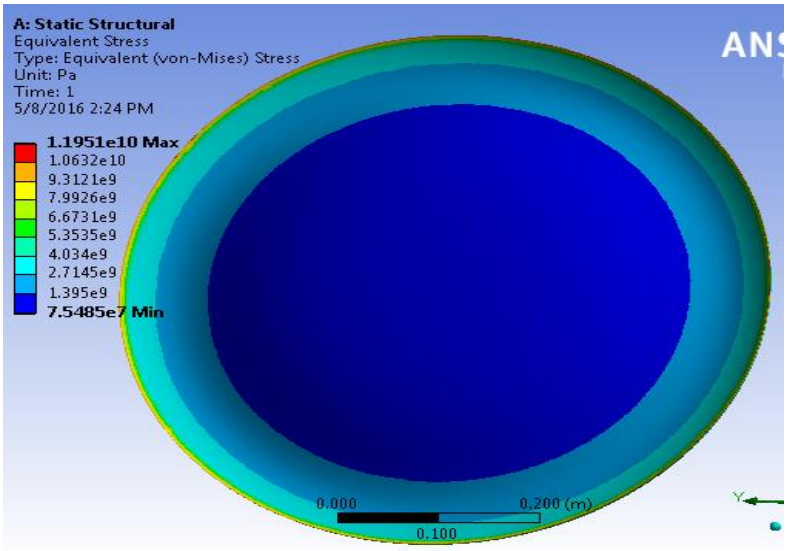

Figure 25: Equivalent Von-Mises Stress at Mach 8

B. Case 2: Thermal Analysis on Kapton for Mach 2 and 8

For the first scenario, the Mach 2 was used with the geometry part body of Kapton had a flexible stiffness behavior. The coordinate system used was set to be default. The reference temperature was set with the environmental conditions. The nonlinear effects were marked as ye and the thermal strain effects also occur. The volume of the entire material is 3.4951e-004 cubic meters with the entire meshing nodes to count for 190546 and elements for 93933. The meshing was set to coarse mesh and the element size was default with a medium smoothing and fast transition and a span angle center of coarse mode. The minimum edge length is said to be 1e-003 meters. The inflation option had a smooth transition with a transition ratio of 0.272 and a maximum layer count of 5 layers with a growth rate of 1.2. The face sizing was set to be performed on all the outer faces of the body open to the analysis window with the element size of 1e-002 meters and a soft behavior. The meshing was also refined among all the faces open to the analysis window. The steady-state thermal initial temperature was taken as 242 Celsius with respect to the value from the table of the survey. The number of steps for the analysis was set to 1 with the step end time to be 1 second. The flux convergence was set to 1e-004 and the solver tolerance of 0.1 W/m^2 and the over relaxation of 0.1. The convection option of the steady state thermal was taken with the frontal convex to be the convection face. The ambient temperature was taken to be the same 242 Celsius. The total and directional heat fluxes are represented below.

Heat flux or thermal flux is the rate of heat energy transfer through a given surface, per unit time. The SI derived unit of heat rate is joule per second, or watt. Heat flux density is the heat rate per unit area. In SI units, heat flux density is measured in [W/m^2]. Heat rate is a scalar quantity, while heat flux is a vector quantity. To define the heat flux at a certain point in space, one takes the limiting case where the size of the surface becomes infinitesimally small. The total heat flux has a maximum of 7.782e09 W/m^2 and an average of 3.4464e-9 W/m^2, the directional heat flux has a maximum of 5.7988e-9 W/m^2 and a normal of 4.8117e-10 W/m^2. The total heat flux defines the total amount of heat energy transfer that can occur with respect to a cross sectional area throughout the body in all directions. The directional heat flux defines the amount of heat transfer of energy with respect to the area in a single direction defined along the central axis of the body.

For the second case, the Mach 8 was used with the geometry part body of Kapton had a flexible stiffness behavior. The coordinate system used was set to be default. The reference temperature was set with the environmental conditions. The nonlinear effects were marked as ye and the thermal strain effects also occur. The volume of the entire material is 3.4951e-004 cubic meters with the entire meshing nodes to count for 190546 and elements for 93933. The meshing was set to coarse mesh and the element size was default with a medium smoothing and fast transition and a span angle center of coarse mode. The minimum edge length is said to be 1e-003 meters. The inflation option had a smooth transition with a transition ratio of 0.272 and a maximum layer count of 5 layers with a growth rate of 1.2. The face sizing was set to be performed on all the outer faces of the body open to the analysis window with the element size of 1e-002 meters and a soft behavior. The meshing was also refined among all the faces open to the analysis window. The steady-state thermal initial temperature was taken as 2669 Celsius with respect to the value from the table of the survey. The number of steps for the analysis was set to 1 with the step end time to be 1 second. The flux convergence was set to 1e-004 and the solver tolerance of 0.1 W/m^2 and the over relaxation of 0.1. The convection option of the steady state thermal was taken with the frontal convex to be the convection face. The ambient temperature was taken to be the same 2669 Celsius. The total and directional heat fluxes are represented below.

Heat flux or thermal flux is the rate of heat energy transfer through a given surface, per unit time. The SI derived unit of heat rate is joule per second, or watt. Heat flux density is the heat rate per unit area. In SI units, heat flux density is measured in [W/m^2]. Heat rate is a scalar quantity, while heat flux is a vector quantity. To define the heat flux at a certain point in space, one takes the limiting case where the size of the surface becomes infinitesimally small. The total heat flux has a maximum of 8.6106e-8 W/m^2 and an average of 5.8369e-8 W/m^2, the directional heat flux has a maximum of 6.4026e-8 W/m^2 and a normal of 5.382e-9 W/m^2. The total heat flux defines the total amount of heat energy transfer that can occur with respect to a cross sectional area throughout the body in all directions. The directional heat flux defines the amount of heat transfer of energy with respect to the area in a single direction defined along the central axis of the body.

The below figures illustrate the temperature distribution for the described situation and parameters above.

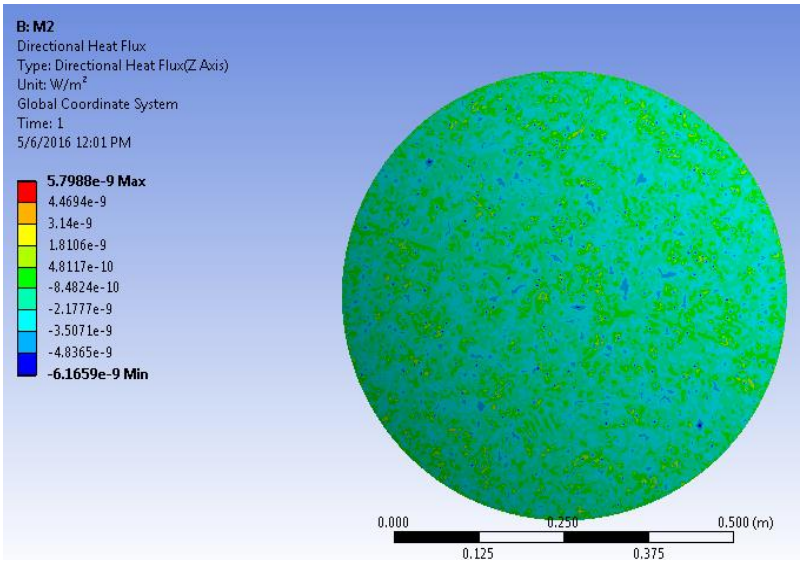

Figure 26: Directional Heat Flux Distribution for Mach 2

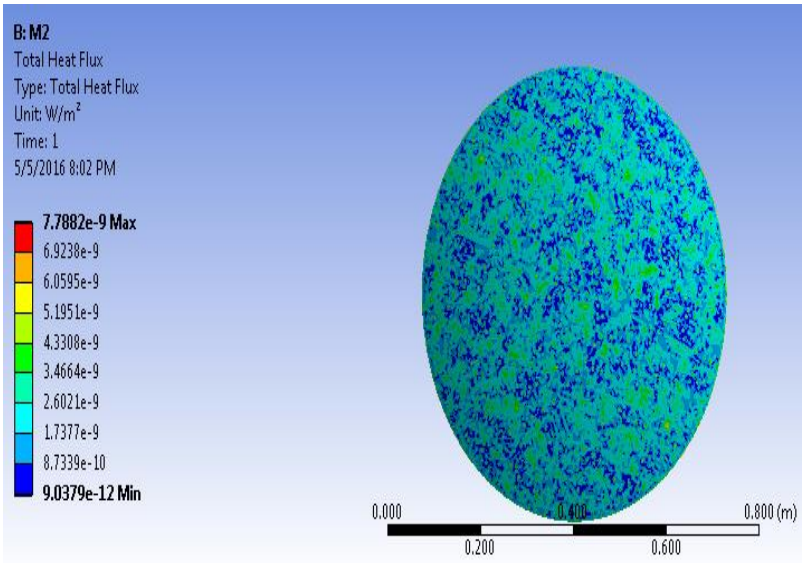

Figure 27: Total Heat Flux Distribution for Mach 2

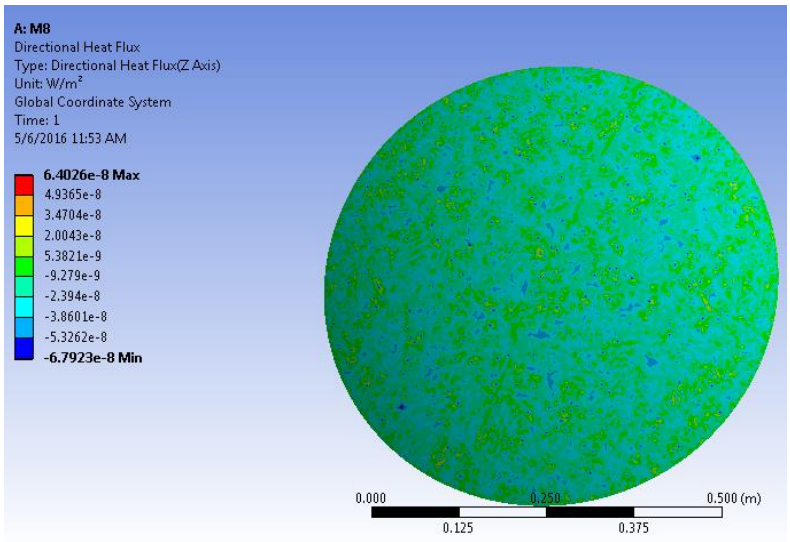

Figure 28: Directional Heat Flux Distribution for Mach 8

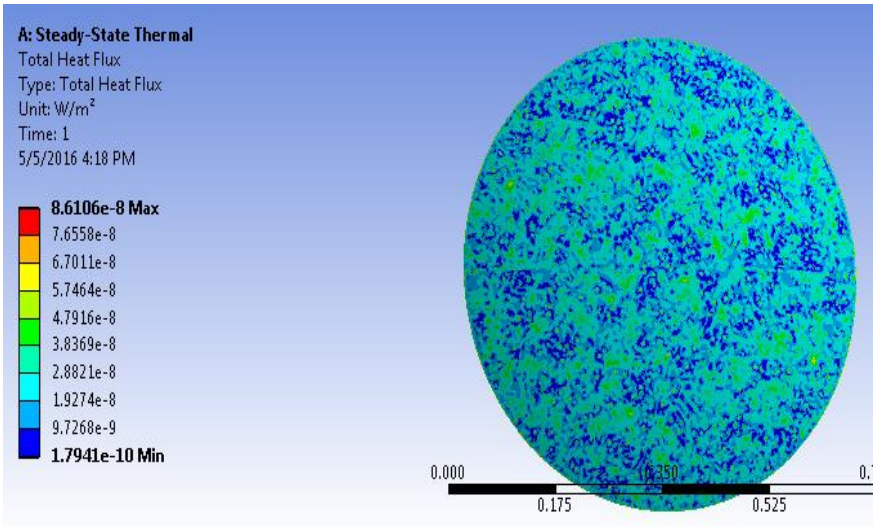

Figure 29: Total Heat Flux Distribution for Mach 8

C. Case 3: Thermo-Structural Analysis on Kapton-Kevlar for Mach 8

The case of re-entry vehicles has both the thermal and the structural stresses acting on it. Since the vehicle is at hypersonic speeds, the high temperatures and high pressures are a concern for the analysis. The thermo-structural analysis serves as a purpose for constructing a model which can withstand the thermal stresses at those conditions specified.

To generate a thermo-structural analysis, two of the ANSYS modes are used, namely the Transient Thermal and Static Structural coupled together to generate the thermo-structural results on the vehicle's aero-shell nose.

In addition, this analysis is performed for the layered Kapton-Kevlar where Kapton is the frontal face covering the Kevlar material. Both the bodies are fixed by a contact of face of the interior of Kapton to the exterior of Kevlar parts designed by CATIA V5. The Kapton layer is taken as a 1 mm gas barrier and the Kevlar layer is taken in the thickness of 5 mm.

The engineering data is set to define all the structural and thermal properties of each of the materials. The geometry was then imported for both the modes.

The first mode to work with is the Transient-Thermal mode. The actual model of the combined layers has a volume of 2.0602e-003 cubic meters. A contact region is verified using the connections tab in the software. Then the mesh is generated with a medium relevance center and a default element size with a medium smoothing. The transition is set to fast and the span angle center is taken as course. The minimum edge length is 1e-003 meters. The refinement is also constructed with the geometry of all the outer surfaces exposed to the window. The face sizing is done in the same way. With this, the meshing of a fine quality is achieved and can be seen by the figure below and a closer figure can be seen below that.

The entire mesh has generated a set of nodes and elements mentioned below along with a table illustrating the entire number of nodes, elements, body elements, and contact elements.

The transient thermal properties have an initial temperature of 2670 Celsius under an analysis setting of 1 step and 1 second of step end time. The initial step time is computed as 1e-002 seconds. The convection phase is provided on the outer face of the combined layer with the film coefficient of 0.12 W/m^2 which is the isotopic thermal conductivity of Kapton. The bottom figures are the results of this thermal-transient analysis

The maximum total heat flux is found to be 1.4823e-8 W/m^2 and the directional heat flux is computed to be nearly 1.581e-9 W/m^2.

With the transient thermal results of the heat flux distribution, the solutions can be used as a set of inputs for generating the static structural analysis. The engineering data would be taken the same. The geometry is positioned by a connecting on the software. The solution phase is connected to the setup phase. The connections and the schematic can be seen by the illustration in the outline section 3.4.

In the static structural phase of the analysis, the meshing and the geometry is the same as the transient thermal phase. Here a pressure of 9.992e+006 Pa is taken with respect to the Mach 8 values taken from the input section. This pressure is

enacted upon the convex section of the combined layer. The physical connection also remains the same as the previous part of this analysis. A fixed support is attached to the rims of the combined layer structure to constitute that this region has another part fixed to the back of this aero-shell. The total setup and the results were computed and the illustrations below represent the distribution of the thermal stresses acted on the aero-shell by both the high temperatures and high pressures. The total static deformation is a maximum at the center and is computed to be 0.2521 meters. The total static elastic strain is computed to be 0.32006.

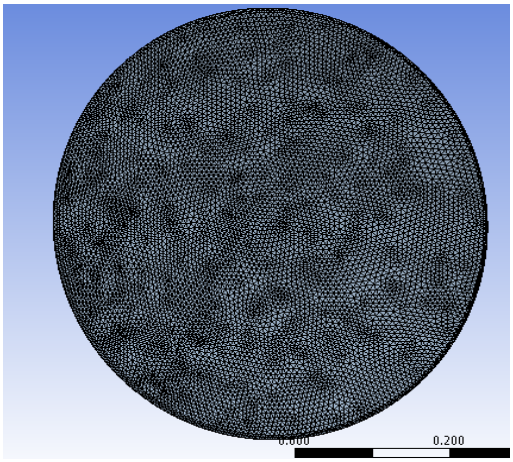

Figure 30: Kapton-Kevlar Mesh

Table 5: Kapton-Kevlar Mesh Summary

TABLE 2—Bodies Summary

Body Name	Nodes	Elements
Kapton	87221	42661
Kevlar	63254	30305

Table 6: Kapton-Kevlar Mesh Summary 2

TABLE 1—FE Model Summary

Description	Quantity
Total Nodes	150475
Total Elements	88494
Total Body Elements	72966
Total Contact Elements	15528

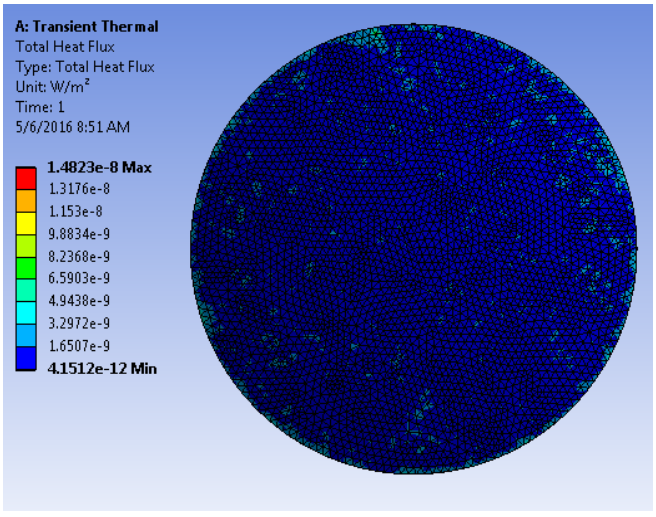

Figure 31: Thermo-Structural Transient Thermal Total Heat Flux Distribution

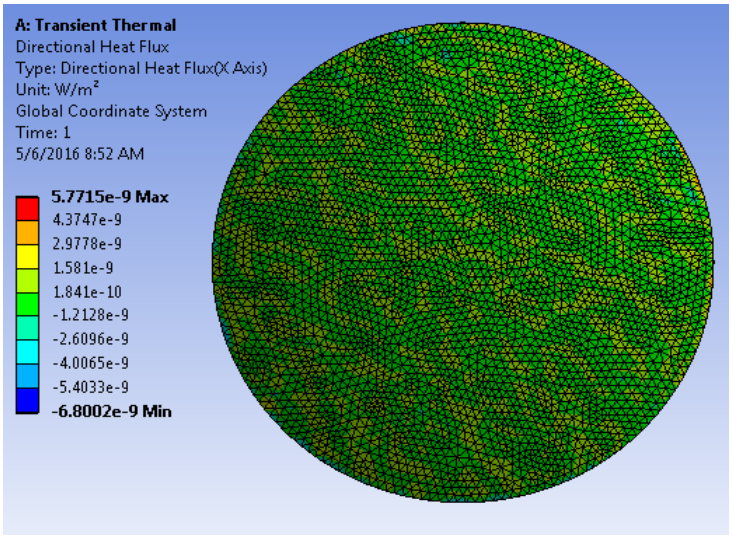

Figure 32: Thermo-Structural Transient Thermal Directional Heat Flux Distribution

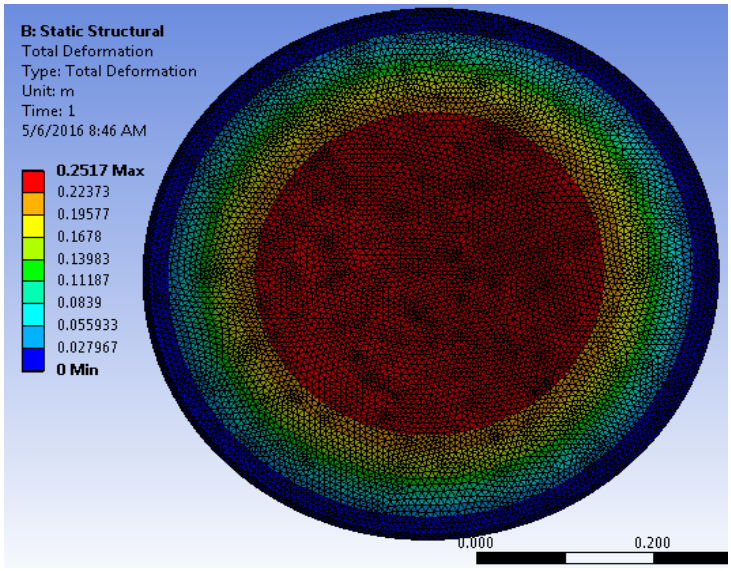

Figure 33: Thermo-Structural Kapton-Kevlar Total Deformation

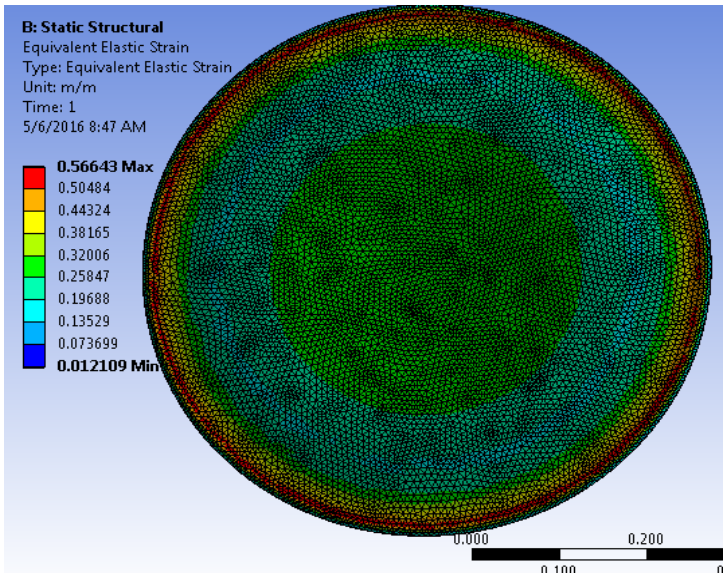

Figure 34: Thermo-Structural Kapton-Kevlar Equivalent Elastic Stress

VII. RESULTS

Before working on the cases, the inputs were taken from the results of a literature survey mentioned in the section 3.4. The resulting graph indicated the Mach numbers and the Stagnation Pressure is plotted on the plane below. [24]

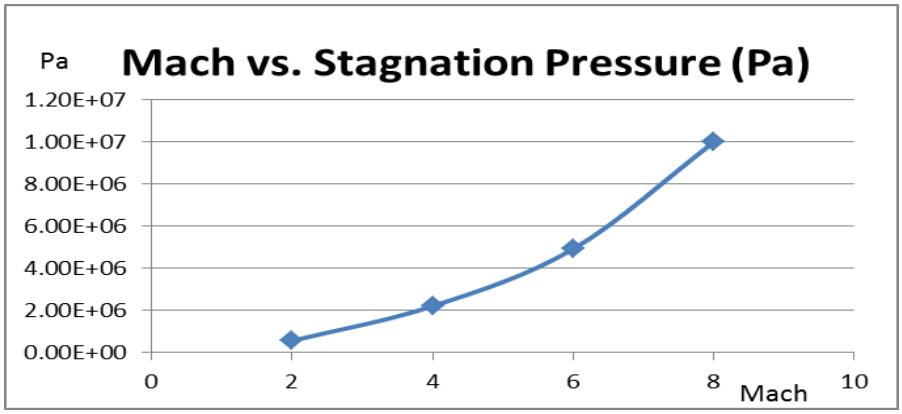

Figure 36: Mach vs. Stagnation Pressure

headings which must not be numbered are "Acknowledgment" and "References".

From this we can see that the Stagnation Pressure values vary exponentially with respect to the Mach numbers because of the ideal isometric equations. As the Mach increases, the rate of growth for the Stagnation Pressure only gets higher. This is mainly due to the shock waves and the impact of the energy of the shocks that occur mainly on the entry segment of any re-entry vehicle.

Case 1:

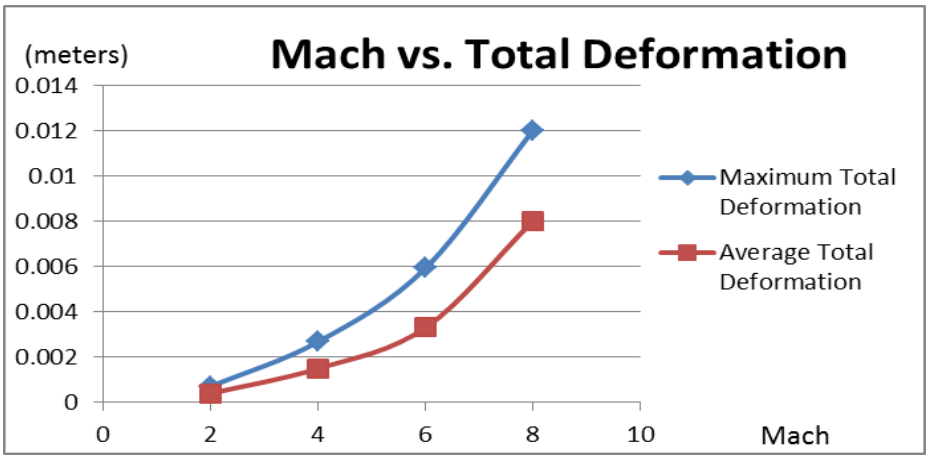

Figure 35: Mach vs. Total Deformation

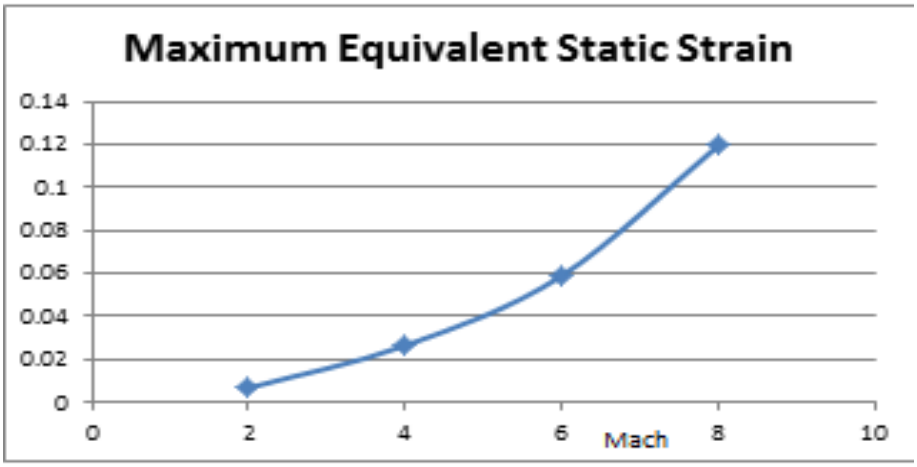

Figure 36: Mach vs. Maximum Equivalent Static Strain

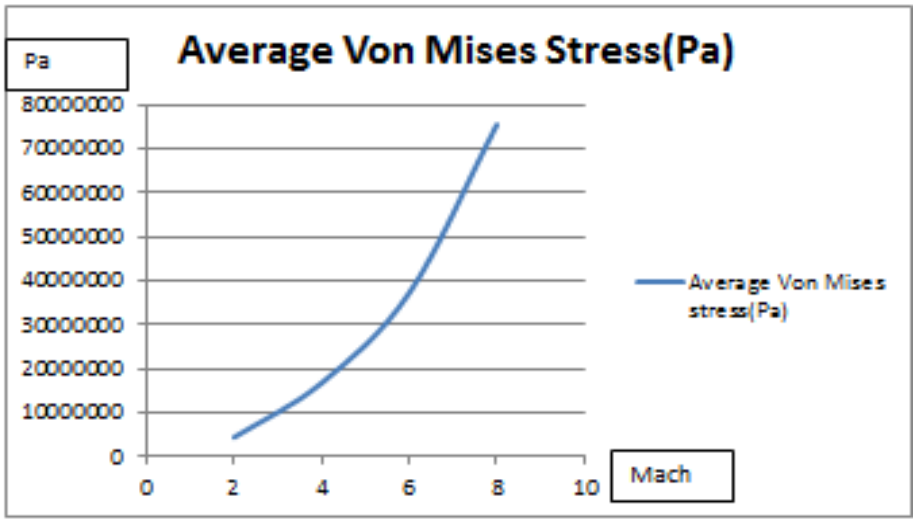

Figure 37: Mach vs. Average Von Mises Stress

The deformation and the equivalent static strain results from the results of the Case 1 are plotted in the above two figures. One can observe that the distribution of the strain and the deformation is very much correlated with the curve from the literature survey. The strain and the deformation are directly proportional to each other. Also we know that the pressure is directional proportional to the strain impacted on it. Thus, as the pressure increases the deformation and the strain increases in the same growth rate as the pressure.

Validation:

$$\frac{P_0}{P} = \left\{\frac{1}{1+\frac{\gamma-1}{2}*M^2}\right\}^{\frac{\gamma}{1-\gamma}} \quad (1)$$

$$\sigma = E * e \quad (2)$$

$$e = \frac{Deformation}{Original\ Length} \quad (3)$$

The equation 1 represents the isometric equation that defines the pressures and the parameters behind shocks and higher Mach numbers. Equation 2 represents the Hooke's Law which states that Stress is directionally proportional to strain with the Young's Modulus defines the rigidity.

P_o → Stagnation Pressure

P → Free Stream Pressure

M → Free Stream Mach Number

γ → Specific Heat Ratio

σ → Stress

E → Young's Modulus

e → Strain

Based on these equations, as the Mach numbers increase, the stagnation pressures increase exponentially with respect to the specific heat ratio. This is when the specific heat ratio and the free stream pressure remain constant. With the increase in the pressure which is actually stress in the case of the Hooke's Law. The pressure (or stress) acts on the object that is a solid. This object has a Young's Modulus, and hence a strain is performed. Since Pressure is directly proportional to strain according to the Hooke's Law. We can say that Strain is directionally proportional in the exponential mode to the Mach number on a re-entry vehicle experiencing higher order Mach numbers. In addition, strain is directionally proportional to the deformation. The following tables are evidence of this calculation and validate this case.

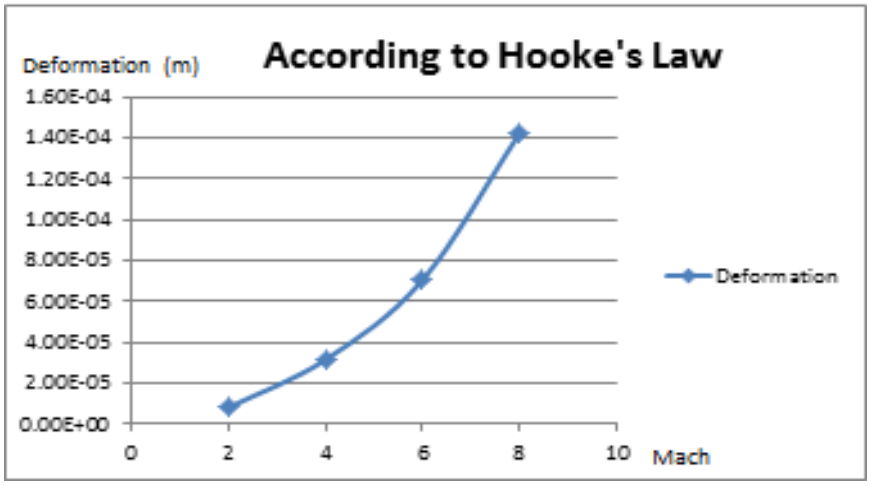

Figure 38: Validation of Hooke's Law Mach vs. Deformation

Case 2:

In the second case, the Kapton material alone is analysed under thermal conditions. This produces the maximum total heat fluxes and the results are tabulated below. Heat flux is given in Watts per squared meters.

Table 7: Case 2 Heat Fluxes values for various Mach Numbers

Mach	**Maximum Total Heat Flux (W/m^2)**	**Average Total Heat Flux (W/m^2)**
2	7.78E+09	3.45E+09
8	8.61E-08	5.84E-08
Mach	**Maximum Directional Heat Flux (W/m^2)**	**Average Directional Heat Flux (W/m^2)**
2	5.80E+09	4.81E-10
8	6.40E-08	5.38E-09

Validation:

The equation below is the heat flux equation.

$$\phi_q = -k\frac{dT(x)}{dx} \quad (4)$$

Here, the negative sign indicates that temperature moves from higher to lower values.

ϕ_q → Heat Flux

k → Thermal Conductivity

dx → Change in the dimensions in the x-axis

Dt → Change in the temperature

At higher Mach numbers, the temperatures analysed are higher. This indicates that the temperature drop is also high from the high initial temperature to the workable temperature of the material. This indicates that, the heat fluxes are also higher in magnitude because the change in temperature is directly proportional to the heat flux.

Case 3:

Table 8: Kapton-Kevlar Thermo-Structural Results

Case 3: Kapton-Kevlar Thermo Structural Results	
Max Total Heat Flux	1.4823e-8 W/m^2
Directional Heat Flux	1.581e-9 W/m^2
Static Total Deformation	0.2521 meters
Static Elastic Strain	0.32006

With the thermo-structural analysis being performed, the above table indicates the results. The high temperatures make metals more prone to deformations because the properties of the material change. In addition, in the non-ideal sense, ablation and ionization occur with the high temperatures causing the material to be more unstable.

VIII. CONCLUSIONS

In conclusion, a segment of the working of a re-entry vehicle (especially HIAD) was studied and performed. This vehicle will be of integral use to us as it has been designed to fulfill its main application to be part of the next Mars mission since the aero-shell of the launch vehicle is limited by fairing and the atmosphere of Mars is too thin to decelerate large masses and limits accessibility to surface altitude. It will give us improved payload access and after inflation it behaves like a rigid device. The aerodynamics is also scalable. The nose was structurally analysed with pressure inputs taken for the following Mach numbers: 2, 4, 6, and 8. The input material used for this purpose was Kevlar and the deformations, elastic strain and Von Mises stresses were obtained. The nose was then thermally analysed with temperature inputs for the following Mach numbers: 2 and 8. The input material used was Kapton, as this material acts as an insulator on the outer surface of the vehicle. Total and directional thermal fluxes were obtained. An assembly of both Kapton and Kevlar was performed and a subsequent thermo-structural analysis was performed for Mach 8. Even though thermo-structural effects are not the only effects on a re-entry vehicle, they are however a major aspect in deciding the entire vehicle's parameters and operating conditions.

The methodology used in this report can be used for various other re-entry vehicles and their analysis. This is important to study their behaviours at various environments including Earth. This helps us design better re-entry vehicles with better materials, better hardware, organized approach, planned mission, and improved safety.

REFERENCES

[1] ANSYS Inc. (2011). ANSYS Parametric Design Language Guide, Release 14.0.

[2] ANSYS, Inc, ANSYS FLUENT 12.0. Theory Guide (2012) URL: http://www1.ansys.com/customer/content /documentation/121/fluent/flth.pdf

[3] Allen, G. A., Jr., Wright, M. J., and Gage, P., "The Trajectory Program (Traj): Reference Manual and User's Guide", NASA TM -2005-212847, 2005.

[4] Askins, P. A., Zell, P. T., and Ross, J. C., "Aerodynamic Decelerator Testing in the National Full-Scale Aerodynamics Complex" AIAA-97-1528, 1997.

[5] Blosser, M.L., "Advanced metallic thermal protection systems for reusable launch vehicles", Doctoral dissertation, Dept. of mechanical and aerospace engineering, University of Virginia, May 2000.

[6] Blosser, M.L, C.J. Martin, D. Kamran, C.C. Poteet (March, 1998) "Reusable Metallic Thermal Protection Systems Development", Third European workshop on thermal Protection Systems, ESTEC, Noordwijk, The Netherlands.

[7] Covington, M.A. (2004). Performance of a Light-Weight ablative thermal protection material for the Stardust Mission sample return capsule. In Proc. 2nd "International Planetary Probe orkshop", Moffett Field, California.

[8] Corneliu Berbente, D. Crunţeanu, D. Racoţi, "On the interpretation of certain thermodynamic expressions and coefficients for ideal gases in terms of average values within temperature intervals", rev. TERMOTEHNICA, No.1/2009, ISSN 1222-4057.

[9] Dec, J.A., Brown, R.D. (2006). An approximate Ablative Thermal Protection System Sizing Tool for Entry System Design. In Proc. 44th AIAA "Aerospace Sciences Meeting and Exhibit", Reno, Nevada.

[10] Fukuoka (2005), Luo Xing et al(2008).Multi-Fidelity Analysis of Corrugated-Core Sandwich Panels for Integrated Thermal Protection Systems.. Department of Mechanical.

[11] Hiroaki Nishikawa, Keiichi Kitamura, Very Simple, carbuncle-free, boundary-layer-resolving, rotated-hybrid Riemann solvers, Elsevier, Journal of Computational Physics, 2008. and Aerospace Engineering, University of Florida.(50th).

[12] Hughes, S. J., Dillman, R. A., Starr, B. R., Stephan, R. A., Lindell, M. C., Player, C. J., Cheatwood, F. M., "Inflatable Reentry Vehicle Experiment (IRVE) Design Overview" 18th AIAA Aerodynamic Decelerator Systems Technology Conference and Seminar, AIAA 2005-1636, Munich, Germany, May 23-26, 2005.

[13] J.-Ch. Robinet, J. Gressier, G. Casalis, J.-M. Moschetta, Shock wave instability and the carbuncle phenomenon: same intrinsic origin?, J. Fluid Mech., Cambridge University Press, 2000 AIAA/ASME/ASCE/AHS/ASC Structures, Dynamics, and Materials Conference, 4 - 7 May 2009.

[14] K. Chul-Soo, Experimental Studies of Supersonic Flow past a Circular Cylinder, Journal of the Physical Society of Japan, 1956.

[15] K.M.Pandey, D.H.Das and B.Acharya, Effects of Variation of Specific Heat on Temperature in Gaseous Combustion with Fluent Software, International Journal of Environmental Science and Development, Vol.1, No.5, December 2010, ISSN: 2010-0264.

[16] Kushner, L. K., Schairer, E. T. "Planning Image-Based Measurements in Wind Tunnels by Virtual Imaging" 49th AIAA Aerospace Sciences Meeting, AIAA 2011-930, Orlando, FL.

[17] Lindell, M. C., Hughes, S. J., Dixon, M., Wiley, C. E. "Structural Analysis and Testing of the Inflatable Re-entry Vehicle Experiment (IRVE), 47th AIAA/ASME/ASCE/AHS/ASC Structures, Structural Dynamics, and Materials Conference, AIAA-2006-1699, May 1-4, 2006.

[18] Milos, F.S., Chen, Y., Squire, T.H. (1999). Updated ablation and thermal response program for spacecraft heatshield analysis. Journal of Spacecraft and Rockets 36(3), 475-483.

[19] Noel Andres Modesto-Madera, A Numerical Study of Supersonic Flow Past A Circular Cylinder, Rensselaer Polytechnic Institute, Hartford, Connecticut, 2010

[20] Oscar Martinez, Satish Bapanapalli, Bhavani Sankar, Raphael Haftka Micromechanical Analysis of Composite Truss-core Sandwich Panels for Integrated Thermal Protection Systems.-. Department of Mechanical and Aerospace Engineering. University of Florida, Gainesville, Florida 32611-6250. (47th AIAA/ASME/ASCE/AHS Structures, structural dynamics, and Materials Conference Conference1 - 4 May 2006, Newport, Rhode Island). (www.aiaa.org).

[21] Satish K, Christian Gogu, Bapanapalli, Bhavani V.Shankar, Raphael T.Haftka (April, 2006), Comparison of Materials for Integrated Thermal Protection Systems for Spacecraft Reentry, AIAA/ASME/ASCE/AHS/ASC Structures, dynamics, And Materials Conference, Honululu, Hawaii.

[22] Satish K, Oscar M.Matrinez, Christian Gogu, Bhavani V.Shankar, Raphael T.Haftka, (May, 2006), Analysis and Design of Corrugated-Core Sandwich Panels for Thermal Protection Systems of Space Vehicles, AIAA/ASME//AHS/ASC Structures, dynamics And Materials Conference, Newport, Rhode Island.

[23] Smith, B. P., Tanner, C. L., Mahzari, M., Clark, I. G., Braun, R. D., Cheatwood, F. M. "A Historical Review of Inflatable Aerodynamic Decelerator Technology Development"

[24] Szasz, Bianca. NUMERICAL STUDY OF COMPRESSIBLE FLOW PAST A REENTRY VEHICLE NOSE. Publication no. 1454-2358. 4th ed. Vol. 75. N.p.: U.P.B Sci. Bull, 2013. Print. D.

[25] Tanner, C. L., Cruz, J. R., Braun, R. D., "Structural Verification and Modeling of a Tension Cone Inflatable Aerodynamic Decelerator" 51st AIAA/ASME/ASCE/AHS/ASC Structures, Structural Dynamics, and Materials Conference, AIAA 2010-2830, Orlando, FL, 12-15 April 2010.

[26] Venkatapathy, E., Laub, B., Hartman, G.J, Arnold, J.O., Wright, M.J., Allen, G.A. (2009). Thermal protection system development, testing, and qualification for atmospheric probes and sample return missions Examples for Saturn, Titan and Stardust-type sample return. Advances in Space Research 44, 138-150.

[27] Williams, S.D., Curry, D.M. (1992). Thermal Protection Materials. Reference Publication 1289, NASA. 3. Tran H.K., et al. (1997). Phenolic Impregnated Carbon Ablators (PICA) as Thermal Protection Systems for Discovery Missions. Technical Memorandum 110440, NASA.

[28] Zang, T., et al "Overview of the NASA Entry, Descent and Landing Systems Analysis Study" AIAA-2010-8649 AIAA SPACE 2010 Conference and Exposition, Anaheim, CA, Aug. 30-Sep 2, 2010.